Analysis of Target Detection Performance for Wireless Sensor Networks

Qing Cao, Ting Yan, John Stankovic, and Tarek Abdelzaher

Department of Computer Science, University of Virginia, Charlottesville VA 22904, USA
{qingcao, ty4k, stankovic, zaher}@cs.virginia.edu

Abstract. In surveillance and tracking applications, wireless sensor nodes collectively monitor the existence of intruding targets. In this paper, we derive closed form results for predicting surveillance performance attributes, represented by detection probability and average detection delay of intruding targets, based on tunable system parameters, represented by node density and sleep duty cycle. The results apply to both stationary and mobile targets, and shed light on the fundamental connection between aspects of sensing quality and deployment choices. We demonstrate that our results are robust to realistic sensing models, which are proposed based on experimental measurements of passive infrared sensors. We also validate the correctness of our results through extensive simulations.

1 Introduction

A broad range of current sensor network applications involve surveillance. One common goal for such applications is reliable detection of targets with minimal energy consumption. Although maintaining full sensing coverage guarantees immediate response to intruding targets, sometimes it is not favorable due to its high energy consumption. Therefore, designers are willing to sacrifice surveillance quality in exchange for prolonged system lifetime. The challenge is to obtain the analytical relationship that depicts the exact tradeoff between surveillance quality and system parameters in large-scale sensor networks. In this paper, we characterize surveillance quality by average detection delay and detection probability of intruding targets. For system parameters, we are mainly concerned with duty cycle and node density. This knowledge answers the question of whether a system with a set of parameters is capable of achieving its surveillance goals.

In this paper, we establish the relationship between system parameters and surveillance attributes. Our closed-form results apply to both stationary and moving targets, and are verified through extensive simulations. Throughout this paper, we adopt the model of unsynchronized duty-cycle scheduling for individual nodes. In this model, nodes sleep and wake-up periodically. Nodes agree on the length of the duty cycle period and the percentage of time they are awake within each duty cycle. However, the wakeup times are not synchronized among nodes. We call this model, *random duty-cycle scheduling*. There are two reasons for this choice. First, random scheduling is probably the easiest to implement in sensor networks since it requires no coordination among nodes. Coordination among nodes takes additional energy and may be severely impaired by clock drifts. Second, many surveillance scenarios pose the requirement of

V. Prasanna et al. (Eds.): DCOSS 2005, LNCS 3560, pp. 276–292, 2005.

stealthiness (i.e., that nodes minimize their electronic signatures). Coordinating node schedules in an ad hoc network inevitably involves some message exchange which creates a detectable electronic signature. In contrast, random scheduling does not require communication. Each node simply sets its own duty-cycle schedule according to the agreed-upon wakeup ratio, and starts surveillance. No extra messages need to be exchanged before a potential target appears. Based on these two considerations, we focus this paper only on random duty-cycle scheduling.

We make two major contributions in this paper. First, for the first time, we obtain closed-form results to quantify the relationship between surveillance attributes and system parameters. The advantage is that we can now answer a variety of important questions without the need for simulation. For example, to decrease the average detection delay for a potential target by half, how much should we increase the node density? In this paper, we demonstrate that this problem, along with many others, can be answered analytically based on our results. Second, we propose a realistic (irregular) model of sensing based on empirical measurements. This model is then incorporated into our simulation to prove the robustness of our analytical predictions. The results show that even under the irregular sensing model, the analytical closed-form results are still quite accurate.

The rest of this paper is organized as follows. Section 2 presents the notations and assumptions of the paper. Section 3 considers stationary target detection. Section 4 addresses mobile target detection. Section 5 presents the irregular sensing model based on experiments. Section 6 discusses related work and Section 7 concludes the paper.

2 Notations and Assumptions

In this section, we present the notations and assumptions for our derivations. First of all, we assume that nodes are independently and identically distributed conforming to a uniform distribution. Density d is defined as the total number of nodes divided by area in which the system is deployed, A_{system}. In our analysis, we adopt a simple sensing model in which a point is covered by a node if and only if the distance between them is less than or equal to the sensing range R of the node. For simplicity, we first assume that all nodes have the same sensing range in all directions. We shall address sensing irregularity in Section 5. Each node is assumed to have a scheduling period T and a duty cycle ratio β, $0 \leq \beta \leq 1$, that defines the percentage of time the node is awake. Each node chooses its wakeup point t_{start} independently and uniformly within $[0, T)$, wakes up for a period of time βT, and then goes back to sleep until $T + t_{start}$. Finally, we assume that (for all practical purposes) the entire system area is covered when all nodes are awake.

Each target in the area moves in a straight line at a constant speed v in our analysis. We assume that all targets are point targets so that their physical sizes can be neglected. Observe, however, that larger targets can still be analyzed by increasing the sensing range used in the analysis by the diameter of the target to account for the larger sensory signature.

3 Stationary Target Sensing Analysis

In this section, we analyze the expected value and probability distribution of detection delay t_d for a stationary, persistent target (e.g., a localized fire).

First, according to our assumptions, since nodes are deployed with a uniform distribution, the number of nodes within an area of πR^2 conforms to a binomial distribution $B(A_{system}d, \pi R^2/A_{system})$. For a sensor network with a reasonable scale, $A_{system}d$ is a large number, and $(A_{system}d)(\pi R^2/A_{system}) = \pi R^2 d$ is a constant, denoted as λ. With these conditions, the binomial distribution can be approximated by a Poisson distribution with parameter λ. Observe that $\lambda = \pi R^2 d$ is the average number of nodes within a sensing range. The probability that there are n nodes covering an arbitrary geometric point is $\frac{\lambda^n}{n!}e^{-\lambda}$, $n = 0, 1, 2, ...$ The probability that no node covers the point (i.e., $n = 0$) is $e^{-\lambda}$. To make this probability smaller than 0.01, λ should be at least $-\ln 0.01 \approx 4.6$. Observe that the detection delay for points that are not covered is infinite, which makes the expected detection delay for the whole area infinitely large. To avoid this problem, we take into account only those points that are covered by at least one node. Our calculations above indicate that as long as there are more than 4.6 nodes on average within a sensing range, the probability that a point is not covered is less than 0.01, which is negligible.

In the rest of the paper, we extensively use two general results from theory of probability. First, if the probability of an event A occurring in a single experiment is p, and if the *number of experiments* conforms to a Poisson Distribution with parameter λ, the probability of event A occurring at least once in the series of experiments is:

$$P = 1 - e^{-p\lambda} \tag{1}$$

In the analysis, we first calculate the probability of detection when the target is covered by one node in a certain area. Since the number of nodes in a certain area conforms to a Poisson distribution, we get the probability that at least one node covers the target.

Another important result relating to our derivation is Proposition 11.6 in [16]: Let X be a nonnegative random variable, then $E(X) = \int_0^\infty P(X > x)dx$.

Since the cumulative distribution function (CDF) of X $cdf(x) = P(X \leq x)$, we have

$$E(X) = \int_0^\infty (1 - cdf(x))dx \tag{2}$$

We will use this fact to derive the average detection delay for both stationary and mobile target detection, after we get the probability that the target is detected within a certain period of time.

Now consider an arbitrary point in the area to be monitored. Suppose node O is the only node covering this point. The duty cycle of node O is shown in Figure 1. Denote the random variable corresponding to the detection delay at this point as t_d. Since the node has a probability β of being awake, we have $P(t_d = 0) = \beta$.

The probability density function (PDF) of t_d $f(\tau)$, where $0 < \tau \leq T - \beta T$, conforms to a uniform distribution, so $f(\tau) = \frac{1}{T}$.
as long as the target can arrive uniformly anywhere within the duty-cycle. Therefore, when there is only one node covering the point, the cumulative probability distribution for the detection delay is:

$$F_{t_d}(\tau) = P(t_d \leq \tau) = \beta + \frac{\tau}{T}, \tag{3}$$

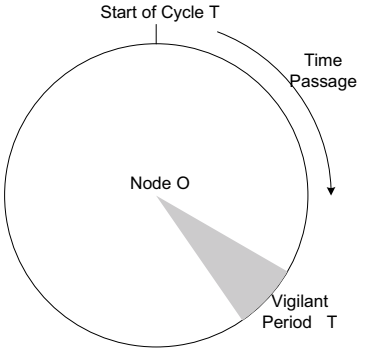

Fig. 1. Duty Cycle of a Particular Node O

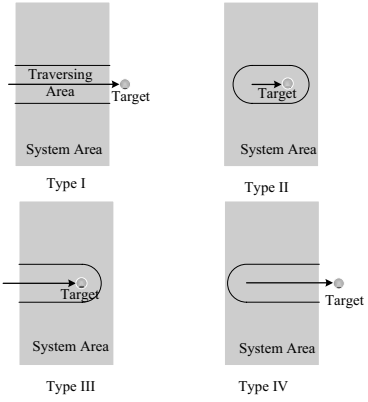

Fig. 2. Target Detection Scenarios

where $0 \leq \tau \leq T - \beta T$. When there are n nodes covering the point, we consider the detection of each node as an experiment. Let event A correspond to the fact that the target is detected within an interval time no larger than t_d. Substituting for the single event probability p in Equation (1) from Equation (3) we get the probability of event A:

$$P(A) = 1 - e^{(\frac{-\lambda\tau}{T} - \beta\lambda)} \tag{4}$$

Since we focus only on those points that are covered, the CDF of detection delay for such points is $P(A)/1 - e^{-\lambda}$, or:

$$F_{t_d}(\tau) = \frac{1 - e^{(\frac{-\lambda\tau}{T} - \beta\lambda)}}{1 - e^{-\lambda}}, 0 \leq \tau \leq T - \beta T \tag{5}$$

where $e^{-\lambda}$ is the probability of voids.

Second, according to Equation (2), the expected value of the delay t_d is:

$$E(t_d) = \int_0^\infty P(t_d > t)dt = \int_0^\infty \frac{e^{-\lambda(\frac{t}{T} + \beta)}}{1 - e^{-\lambda}} dt = \frac{T}{\lambda} e^{-\beta\lambda}/(1 - e^{-\lambda}) \tag{6}$$

In particular, when the duty cycle β approaches 0 and $1 - e^{-\lambda}$ approaches 1, Equation (6) turns into T/λ. Therefore, we conclude that when the duty cycle is sufficiently small and the density is sufficiently large, the average detection delay is inversely proportional to node density.

4 Mobile Target Sensing Analysis

In this section, we analyze the detection delay for mobile targets. We consider a target that moves at velocity v along a straight path, and consider four detection scenarios, as shown in Figure 2. We categorize these scenarios based on whether or not the start or end point of the target path is inside the system area. For target scenarios of type I

and type IV (where the end-point is outside the monitored area), we are interested in the probability that the target is detected by at least one node before it leaves the area. For target scenarios of type II or type III (where the end-point is inside the monitored area), we are interested in the expected time and distance the target travels before it is detected. The system area is assumed to be rectangular, in which nodes are randomly deployed. The target is detected within a radius R (or diameter $2R$) which constitutes the width of the traversing areas shown in Figure 2. We focus on type I and type II scenarios, and outline the results for the other two types.

We demonstrate a more detailed model for type II target detection in Figure 3 (type I model is similar). Consider the traversing area S consisting of the rectangle and two half-circles in the figure. For a potential target that travels from point A to point B (where distance $AB = L$), only nodes located within this area can detect the target, for example, node M, which has an intersection length of l with the target's moving track. Therefore, we call this area the detection area. Since all nodes are deployed conforming to a uniform distribution, the number of nodes in the detection area also conforms to Poisson Distribution approximately. According to Equation (1) mentioned above, in order to find the probability of detection, we only need to find the detection probability when there is only one node within this area.

Now consider node M. Since it has an intersection length with the target track, the potential target takes time l/v to pass its sensing area. Therefore, the target appears to be a temporary event with a lifetime of l/v to node M, which means it has a probability of $\min(\beta + \frac{l}{vT}, 1)$ to be detected by node M. Considering that node M could be anywhere within the detection area, we now analyze the average detection probability for node M to detect the target.

Notice that $\beta + \frac{l}{vT}$ can be at most 1, and if it is, the target will definitely be detected when it passes. This fact categorizes potential targets into two types, fast and slow. For fast targets, the expression $\beta + \frac{l}{vT}$ is always smaller than or equal to 1. Therefore, we can obtain the expectation of detection delay directly by integrating over the detection area. On the other hand, if v is small enough, $\beta + \frac{l}{vT}$ can become larger than 1, thus, we have to partition the detection area first before the integral. Observe that the maximal intersection length between the target path and a sensor's range is $2R$. Therefore, if target velocity $v \geq \frac{2R}{(1-\beta)T}$, then $\beta + \frac{l}{vT}$ is always smaller than or equal to 1. We use $\frac{2R}{(1-\beta)T}$ as the threshold between fast and slow targets.

4.1 Detection Analysis for Fast Targets

For a fast target we can express the probability that the target is detected given there is only one node in the detection area, S, as follows:

$$P = \int_S (\beta + \frac{l}{vT}) ds/S = \beta + \frac{\int_S l ds}{vTS} \tag{7}$$

Thus, we only need to calculate $\int_S l ds$ and S.

Because of symmetry, we only need to calculate the integral $\int_S l ds$ within the first quadrant, as shown in Figure 4.

For a type I target, we need to do the integral over area A and B, while for a type II target, we need to do the integral over A, B and C.

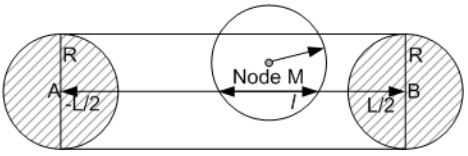

Fig. 3. Target Detection Example

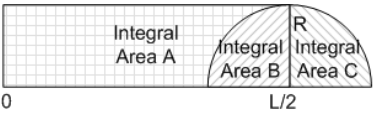

Fig. 4. Fast Target Detection

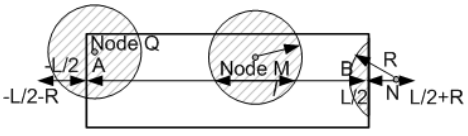

Fig. 5. Fast Target Detection Illustration

Fast Type I Target Analysis. For a type I target, the area under consideration consists of area A and B. Therefore, we have:

$$\int_{S_{A+B}} lds/S_{A+B} = \frac{\phi_A + \phi_B}{LR/2} \tag{8}$$

while

$$\phi_{A+B} = \int_0^R dy \int_0^{\frac{L}{2}} 2\sqrt{R^2 - y^2} dx = \frac{\pi R^2 L}{4} \tag{9}$$

Thus, we get the overall probability as:

$$P = \beta + \frac{\pi R^2 L}{2RLvT} = \beta + \frac{\pi R}{2vT} \tag{10}$$

Fast Type II Target Analysis. Similar to the type I target analysis, we have:

$$\int_{S_{A+B+C}} lds/S_{A+B+C} = \frac{\phi_A + \phi_B + \phi_C}{LR/2 + \pi R^2/4} \tag{11}$$

Therefore,

$$\phi_A = \int_0^R dy \int_0^{\frac{L}{2} - \sqrt{R^2 - y^2}} 2\sqrt{R^2 - y^2} dx = \frac{\pi R^2 L}{4} - \frac{4R^3}{3} \tag{12}$$

$$\phi_B = \int_0^R dy \int_{\frac{L}{2} - \sqrt{R^2 - y^2}}^{\frac{L}{2}} (\frac{L}{2} + \sqrt{R^2 - y^2} - x) dx = R^3 \tag{13}$$

$$\phi_C = \int_0^R dy \int_{\frac{L}{2}}^{\frac{L}{2} + \sqrt{R^2 - y^2}} (\frac{L}{2} + \sqrt{R^2 - y^2} - x) dx = \frac{R^3}{3} \tag{14}$$

Thus, we get the overall probability as:

$$P = \beta + \frac{\pi R^2 L}{(2RL + \pi R^2)vT} = \beta + \frac{\pi RL}{(2L + \pi R)vT} \tag{15}$$

Note that for the case $L < 2r$, the derivation is a little different. However, the result remains the same and for simplicity we omit the details of derivation.

We also have a more intuitive explanation for the calculation of $\int_S lds$. This expression is an integral of a line segment of length l on the target's locus for each point p in the traversing area S. Note that a point p' belongs to the line segment if and only if its distance from p is smaller or equal to R, the sensing range. Therefore, the integral $\int_S lds$ is equivalent to the integral $\int_L sdl$, where L is the locus of the target, and s is the area in which each point has a shorter distance than R to dl. For type II targets, s is simply πR^2 and therefore $\int_S lds$ is simply $\pi R^2 L$, which verifies Equation (15). It is a little more complicated for type I targets since s can be smaller than πR^2. For example, for point N in Figure 5, s is a half-lens. The expression then becomes the integral of the overlapping area of the circular disk with radius R and the traversing area over L. We can think it as a circular disk virtually moving from $-L/2-R$ to $L/2+R$ and calculate the accumulation of overlapping areas. To make the calculation simpler, equivalently, we can also imagine a fixed circular disk and virtually move the traversing area and calculate the accumulation overlapping areas. This also gives a result of $\pi R^2 L$, which verifies Equation (10).

4.2 Detection Analysis for Slow Targets

Now consider $v < \frac{2R}{(1-\beta)T}$. The main difference in this case is that it is possible that for certain node positions (x, y), $l(x, y) > (1 - \beta)vT$, therefore $p(x, y)$ is 1 instead of $\beta + l(x, y)/vT$. Suppose there are two partitions, U and V. In U, $p(x, y) = \beta + l(x, y)/vT$, and in V, $p(x, y) = 1$. Therefore, we have:

$$\begin{aligned} P &= \frac{\int_{S_U}(\beta + \frac{l}{vT})ds + \int_{S_V} 1}{S_{A+B}}ds = \frac{\int_{S_{U+V}}(\beta + \frac{l}{vT})ds + \int_{S_V}(1 - \beta - \frac{l}{vT})ds}{S_{U+V}} \\ &= \beta + \frac{\int_{S_{U+V}} lds}{(S_{U+V})vT} + \frac{S_V(1 - \beta) - \int_{S_V} lds/vT}{S_{U+V}} \end{aligned} \tag{16}$$

Obviously, the term $\beta + \frac{\int_{S_{U+V}} lds}{(S_{A+B})vT}$ is exactly what we have obtained for fast object analysis. So now we need to calculate $S_V(1 - \beta)$ and $\int_{S_V} l$. We classify the analysis into two cases according to type I and type II targets.

Slow Type I Target Analysis. In this type, the partition where $p(x, y) = 1$ is the rectangle area A in Figure 6. We define another variable a such that $\beta + 2a/vT = 1$. The height of the rectangle is $\sqrt{R^2 - a^2}$.

Observing that $\frac{S_V(1-\beta)-\int_{S_V} lds/vT}{S_{U+V}} = \frac{\int_{S_V}[(1-\beta)vT-l(x,y)]dxdy}{S_{U+V}vT}$. Therefore, we have:

$$\int_V [(1 - \beta)vT - l(x, y)]dxdy = \int_A [2a - l(x, y)]dxdy \tag{17}$$

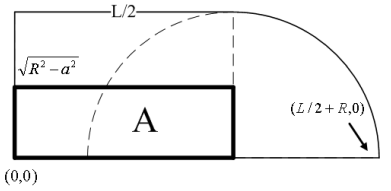

Fig. 6. Type I target Detection

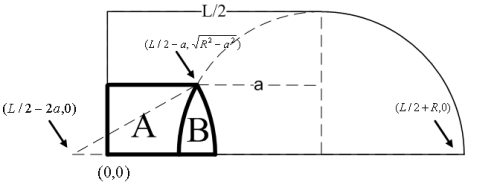

Fig. 7. Regions A and B

in which

$$\iint_A [2a - l(x,y)]dxdy = \int_0^{\sqrt{R^2-a^2}} \int_0^{\frac{L}{2}} (2a - 2\sqrt{R^2-y^2})dxdy$$

$$= \int_0^{\sqrt{R^2-a^2}} [aL - L\sqrt{R^2-y^2}]dy = aL\sqrt{R^2-a^2} - L(\frac{a\sqrt{R^2-a^2}}{2} + \frac{R^2}{2}sin^{-1}\frac{\sqrt{R^2-a^2}}{R})$$

$$= [aL\sqrt{R^2-a^2} - LR^2 sin^{-1}\frac{\sqrt{R^2-a^2}}{R}]/2$$

Therefore we obtain:

$$\iint_A [2a - l(x,y)]dxdy = Lk(R,a)/4 \tag{18}$$

where

$$k(R,a) = 2a\sqrt{R^2-a^2} - 2R^2 cos^{-1}(\frac{a}{R}) \tag{19}$$

Finally, we get when $L \geq 2R$, $v < \frac{2R}{(1-\beta)T}$, for a type I target,

$$P = \beta + \frac{\pi R^2 + k(R,a)}{2RvT} \tag{20}$$

Slow Type II Target Analysis. In this type, the partition where $p(x,y) = 1$ is less regular. We still define a such that $\beta + 2a/vT = 1$. Observe that Figure 7 plots the region where $p(x,y) = 1$, which includes A and B, whose boundaries are formed by line $y = \sqrt{r^2-a^2}$ and two circles which centered at $(L/2 - 2a, 0)$ and $(L/2, 0)$, respectively. For $(x,y) \in A \cup B$, $p(x,y) = 1$.

Similarly, we have:

$$\int_V [(1-\beta)vT - l(x,y)]dxdy = \int_{A+B} [2a - l(x,y)]dxdy \tag{21}$$

in which

$$\iint_A [2a - l(x,y)]dxdy = \int_0^{\sqrt{R^2-a^2}} \int_0^{\frac{L}{2}-\sqrt{R^2-y^2}} (2a - 2\sqrt{R^2-y^2})dxdy$$

$$= \int_0^{\sqrt{R^2-a^2}} (\frac{L}{2} - \sqrt{R^2-y^2})(2a - 2\sqrt{R^2-y^2})dy$$

$$\iint_B [2a - l(x,y)]dxdy = \int_0^{\sqrt{R^2-a^2}} \int_{\frac{L}{2}-2a+\sqrt{R^2-y^2}}^{\frac{L}{2}-\sqrt{R^2-y^2}} [2a - (\sqrt{R^2-y^2} - \frac{L}{2} - x)]dxdy$$

$$= \int_0^{\sqrt{R^2-a^2}} [(2a - \sqrt{R^2-y^2} - \frac{L}{2})(2\sqrt{R^2-y^2} - 2a) + 2a^2 - aL - 2a\sqrt{R^2-y^2} + L\sqrt{x^2-y^2}]dy$$

Therefore we can obtain:

$$\iint_{A+B} [2a - l(x,y)]dxdy = (L-2a)k(R,a)/4$$

where

$$k(R,a) = 2a\sqrt{R^2-a^2} - 2R^2 cos^{-1}(\frac{a}{R}) \tag{22}$$

Finally, we get when $L \geq 2R$, $v < \frac{2R}{(1-\beta)T}$, for a type II target,

$$P = \beta + \frac{\pi R^2 L + (L-2a)k(R,a)}{(2RL + \pi R^2)vT} \tag{23}$$

Indeed, in Figure 7, we only plotted the case where $2a > R$. For $2a < R$, the derivation is similar, and the results are the same.

When $a = 0$, $k(R,a) = -\pi R^2$. When $a = R$, $k(R,a) = 0$. We also have

$$\frac{\partial k(R,a)}{\partial a} = 4\sqrt{R^2-a^2} \geq 0, \tag{24}$$

so $k(R,a)$ is a monotonically non-decreasing function of a. Interestingly, the area of B is exactly $-k(R,a)/2$.

Denote $m(R,\beta)$ as the function substituting a with $(1-\beta)vT/2$ in $k(R,a)$, then

$$m(R,\beta) = (1-\beta)vT\sqrt{R^2 - \frac{(1-\beta)^2v^2T^2}{4}} - 2R^2\cos^{-1}[\frac{(1-\beta)vT}{2R}] \tag{25}$$

$m(R,\beta)$ is a monotonically non-increasing function of β. When $\beta = 1 - \frac{2R}{vT}$, $m(R,\beta) = 0$. When $\beta = 1$, $m(R,\beta) = -\pi R^2$.

Additionally, for a slow type II target, if the travel distance L is less than $(1-\beta)vT$, the detection probability for a node located within the detection area cannot be larger than 1. Therefore, we should treat this period of time in the same way as a fast target. Therefore, we can revise the final probability as:

$$P = \beta + \frac{\pi R^2 L + min((L-2a)k(R,a), 0)}{(2RL + \pi R^2)vT} \tag{26}$$

Average Detection Delay and Probability. So far, we have finished the derivation of $P(L,v)$ for both slow and fast objects. Next we find the detection probability for a type I target, and average detection delay for a type II target.

First, consider fast targets. According to Equation 1, for a fast type I target, with a deployment width of L, we obtain the detection probability as follows:

$$P_{detection}(v) = 1 - e^{-2RLdP} = 1 - e^{-2RLd(\beta + \frac{\pi R}{2vT})} \tag{27}$$

while for slow targets, the result is:

$$P_{detection}(v) = 1 - e^{-2RLdP} = 1 - e^{-2RLd(\beta + \frac{\pi R^2 + k(R,a)}{2RvT})} \tag{28}$$

For fast type II targets, the cumulative distribution function of the detection delay t_d is:

$$F_{t_d}(t) = P(t_d \le t) = 1 - e^{-d(2Rvt+\pi R^2)(\beta + \frac{\pi Rvt}{(2vt+\pi R)vT})} \tag{29}$$

While for slow targets, the function is:

$$F_{t_d}(t) = P(t_d \le t) = 1 - e^{-d(2Rvt+\pi R^2)(\beta + \frac{\pi R^2 vt + min(0,(vt-2a)k(R,a))}{(2Rvt+\pi R^2)vT})} \tag{30}$$

For fast targets, the expected detection delay is

$$E(T_d) = \int_0^\infty e^{-\beta\pi R^2 d - vt(2R\beta + \frac{\pi R^2}{vT})d} dt = \frac{e^{-\beta\pi R^2 d}}{(2R\beta v + \frac{\pi R^2}{T})d} \tag{31}$$

Similarly, when $v < \frac{2R}{(1-\beta)T}$, the expected detection delay is[1]:

$$\begin{aligned} E(T_d) =& \int_0^{2a} e^{-\beta\pi R^2 d - vt(2R\beta + \frac{\pi R^2}{vT})d} dt + \int_{2a}^\infty e^{-\beta\pi R^2 d + \frac{2ak(R,a)d}{vT} - vt(2R\beta + \frac{\pi R^2 + k(R,a)}{vT})d} dt \\ =& \frac{e^{-\beta\pi R^2 d}}{(2R\beta v + \frac{\pi R^2}{T})d}[1 - \frac{m(R,\beta)e^{-(2R\beta vT + \pi R^2)(1-\beta)d}}{2R\beta vT + \pi R^2 + m(R,\beta)}] \end{aligned} \tag{32}$$

4.3 Summary

So far, we have explained in detail the derivation for type I and type II targets in this paper. The authors have also finished the derivation of the detection delay and probability for type III and IV targets, using a similar derivation approach. Due to space limitations, we only outline our final results for type III and type IV targets, as follows:

Expected detection delay for fast type III targets:

$$E(T_d) = \frac{e^{-\beta\pi R^2 d/2}}{(2R\beta v + \frac{\pi R^2}{T})d} \tag{33}$$

Expected detection delay for slow type III targets:

$$E(T_d) = \frac{e^{-\beta\pi R^2 d/2}}{(2R\beta v + \frac{\pi R^2}{T})d}[1 - \frac{m(R,\beta)e^{-(2R\beta vT + \pi R^2)(1-\beta)d/2}}{2R\beta vT + \pi R^2 + m(R,\beta)}] \tag{34}$$

Detection probability for fast type IV targets:

$$P = 1 - e^{-(2RL + \pi R^2/2)d(\beta + \frac{\pi RL}{(2L+\pi R/2)vT})} \tag{35}$$

Detection probability for slow type IV targets:

$$P = 1 - e^{-(2RL + \pi R^2/2)d(\beta + \frac{\pi R^2 L + min((L-a)k(R,a),0)}{(2RL+\pi R^2/2)vT})} \tag{36}$$

[1] Observe that if $v = 0$ (this is equivalent to a stationary target), we obtain the expected delay to be ∞. This is because we do not exclude voids in the mobile target model, and the existence of voids leads to infinitely large expected detection delay in stationary target detection.

4.4 Discussion

We now discuss the implications of our analytical results. First, we assume that almost all of the area is covered, that is, $1 - e^{-\lambda} \approx 1$, thus, $\lambda \geq 4.6$ according to our earlier discussion. Second, in order to save energy, we assume that β approaches 0, that is, the waking period is sufficiently small compared with the total scheduling period. Based on these two assumptions, we have several interesting observations.

First, for fast type I target detection, Equation (27) can be simplified to $1 - e^{-\frac{\lambda}{vT}L}$. Therefore, in order to obtain 99% detection probability, we have $L \geq \frac{4.6vT}{\lambda}$. Assume $\lambda \approx 4.6$, $L \geq vT$. The result is quite intuitive: in order to almost certainly catch an intruding target, the deployment width can be no smaller than the product of the target velocity and the scheduling period.

Second, for a fast type II target, Equation (29) can be simplified to $1 - e^{-\frac{\lambda t}{T}}$. This means that for a target that starts from within the system area, the probability of being caught increases exponentially. Also, to make this probability larger than 99%, $t \approx T$, given that λ is 4.6. This result is also confirmed in our simulations.

Third, for a type II target, the detection delay can be simplified as T/λ if β approaches 0. This result is the same as the stationary detection delay, which means that as β approaches 0, regardless of the movement pattern of the target, the detection delay is approximately constant, determined only by the scheduling period and node density.

4.5 Simulation-Based Verification

We now demonstrate that the derivation results are consistent with simulation results under perfect circular range assumptions. In the first set of simulations of stationary targets, locations of nodes are generated conforming to a uniform random distribution over a unit area with size $100m \times 100m$, without loss of generality. The period T is chosen to be $1s$. The waking points of the nodes are generated according to a uniform distribution over $[0s, 1s]$. The sensing range for circular model is $10m$. We choose a point $(50, 50)$ and generate $10,000$ sets of random target locations to run the simulations. The parameter $\lambda = \pi r^2 d$ is set to 5. We record the number of experiments where the detection delay is smaller than or equal to $0s$, $0.05s$, $0.10s$, ..., $0.90s$, and $0.95s$. We then compare these frequencies with the cumulative distribution functions (CDF's) obtained in the analysis section. The simulation results are shown in Figure 8. From the figure we can see that our analysis and simulation results match well.

In the second set of simulations, we choose various λ values (5, 7, 9 and 11) and β values (0, 0.1, 0.2, ..., 1), and run simulations to gather the average detection delays. Other settings are the same as the previous set. We compare the average detection delays with the theoretical expected detection delays obtained in the analysis section and plot Figure 9. The figure shows that the average delays are very close to the analytical expected delays.

The settings for simulation verification with mobile target tracking are the same as the stationary setting, except that now the target has a velocity. We only consider type II target detection in this section. Other types can be similarly verified. The simulation result is shown in Figure 10. Observe that velocity $2.5m/s$ means a slow target, according to our threshold. In particular, its cumulative detection probability has a relatively long tail, compared to the distribution of targets with higher velocity, implying that for slower

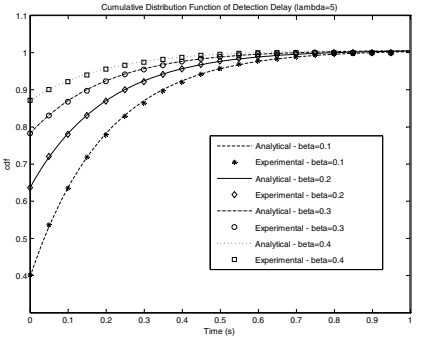

Fig. 8. Stationary Detection Delay Distribution

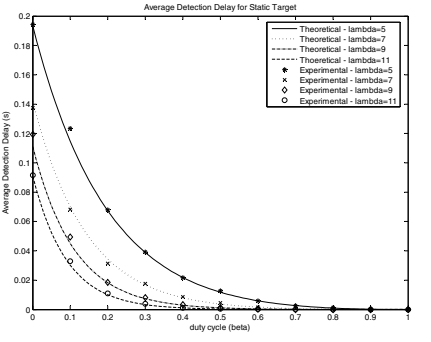

Fig. 9. Average Stationary Detection Delay

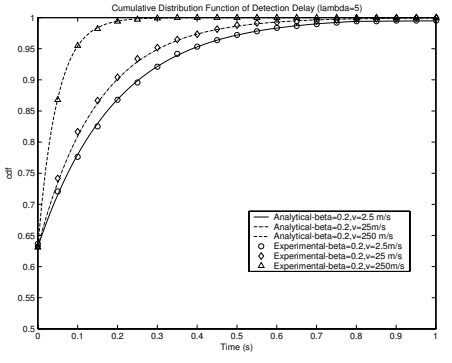

Fig. 10. Mobile Detection Delay Distribution

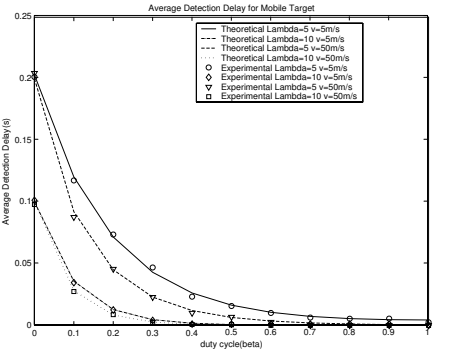

Fig. 11. Average Mobile Detection Delay

targets, there is a higher chance for the target to remain undetected after the scheduling cycle T. Again, we observe that our analysis and the simulation results match well.

In the second set of simulations, we choose various λ values (5 and 10), velocity ($5m/s$ and $50m/s$), and β values (0, 0.1, 0.2, ..., 1), and run simulations to gather the average detection delays. Other settings are the same as in the previous set. We compare the average detection delays with the theoretical expected detection delays obtained in the analysis section and plot Figure 11. The figure shows that the average delays are very close to the analytical expected delays.

The simulation results demonstrate the viability of using our results to predict the system performance. For example, suppose that we have a deployment of $\lambda = 5$ and $T = 1s$, in order to make sure that the expected detection delay to be no larger than $0.1s$, we can calculate that β must be at least 0.14. The simulation results confirm this calculation (Figure 9).

5 Practical Application

An example application of random duty-cycle sensor networks is a surveillance system that tracks trespassers. A person is detected by motion sensors. Once such an event is

triggered, the detecting node sends a wakeup command to its neighbors to track the intruder. These commands constitute messages with a preamble that is longer than the duty-cycle period T. Thus, all neighbors eventually wake up and receive the message. It alerts them to remain awake and track, possibly waking up their neighbors as well. Subsequent detections from multiple sensor nodes eventually reconstruct the target's path. Other types of sensors, such as magnetic ones, can be applied to tell if the person carries a weapon.

5.1 Application Analysis and Sensing Irregularity

We simulate the aforementioned application and check whether simulation results match analytical predictions. However, our discussions so far have assumed a perfectly circular sensing model. This assumption makes the analysis tractable, and leads to closed-form results. Real sensing devices used in this application do not have such a perfect sensing area. In experiments, we use passive infrared sensors (PIR sensors) as motion sensors, and identify the causes of irregular sensing range. We then propose a realistic sensing model for PIR sensors. We integrate this model into our simulations and show that the predictions based on our analysis are quite robust under realistic sensing irregularities.

We have PIR sensors installed on the ExScal XSM motes from OSU and Cross-Bow [6]. At present, four motion sensors are integrated on a single ExScal Mote to provide a 360 degree surveillance range (each individual motion sensor can only handle a 90 degree area). We carried a series of experiments on ExScal nodes. Specifications of ExScal nodes can be found at [1].

5.2 Experimental Results

In principle, PIR sensors can detect anything that generates an infrared field disturbance, such as vehicles, persons, etc. We are interested in the ability of PIR sensors to detect walking persons, as demanded by the application. The central metric is sensing range of PIRs. In individual tests, we let a person walk by at different distances and angles relative to the sensing node, and measure the maximal range of detection. All experiments are repeated in an open parking lot. We program the node with a simple frequency analysis procedure to report events. The procedure relies on an adaptively adjusted threshold to compare the current readings. The main purpose of this adaptive threshold is to avoid false alarms introduced by weather changes, since this change can produce infrared noise that may trigger the sensor. More specifically, our procedure monitors the average readings of the filtered signal within a moving window. If the average reading observed is much smaller than the current threshold, it decreases the

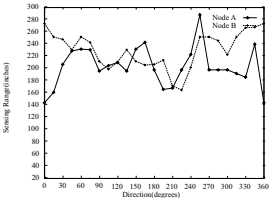

Fig. 12. Range with Directions

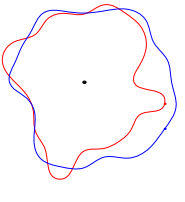

Fig. 13. Ranges of Two Nodes

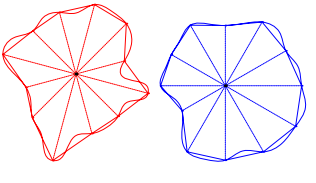

Fig. 14. Range Approximations

threshold by taking a weighted average. On the other hand, if the average energy is close to or larger than the threshold for a certain period, the sensor decides that the weather is noisy, and increases the threshold. Practically we are able to filter out almost all false alarms using this technique. We note that this technique also filters out those slight disturbances that may, in fact, be caused by the target. Thus, the results proposed below present effective sensing range in slightly noisy environments, which are different from precisely controlled environments.

We measured the sensing range from 24 equally divided directions. At each direction, a person moves with different distances from the sensor node. If the fluctuation of the filtered sensor reading exceeds a predefined noise threshold due to the nearby motion, the measured point is within the sensing range. If the motion does not cause a fluctuation greater than the threshold, the measured point is out of the sensing range. In the experiments we found out that the sensitivity of the sensors changes dramatically at the edge of the sensing range. The motion can always be detected in the sensing range and the motion 10 inches beyond the sensing range never triggers the sensors. Therefore, the precision of the range measurement is always within 10 inches (the range itself being hundreds of inches). The experimental results for two representative nodes are shown in Figure 12. Obviously, with four sensors, the range is far from being circular. A more intuitive illustration is shown in Figure 13, where the sensing range in each direction is plotted to scale.

Based on the experimental results of multiple tests, we have the following observations regarding the PIR sensing capability. First, the sensing range of one node is not isotropic, that is, the node exhibits different ranges in different directions. Second, the boundary of the sensing range is delineated quite sharply, with predictably no detection when the range is exceeded by about 3-7%. Third, we can consider the variation of ranges relatively continuous. We do observe sudden changes in the sensitivity of some nodes, but this is very uncommon. Therefore, a model may consider connecting sensitivity ranges in different directions using continuous curves. Fourth, the sensing range distribution in different directions roughly conforms to a Normal Distribution. This conclusion is based on statistical analysis of our experimental data using a Kolmogorov-Smirnov Test [24]. We concluded from our experimental data set that the sensing range in one direction can be approximated with a Normal Distribution with an expectation of 217 inches and a standard deviation of 32 inches.

5.3 Realistic Sensing Model for PIR sensors

In this section, we present a realistic sensing model for PIR nodes. This model is designed to reflect the three key observations: non-isotropic range, continuity and normality. First, the model determines sensing ranges for a set of equally-spaced directions. Each range can either be specified based on actual measurements or obtained from a representative distribution, for example, the normal distribution $N(217, 32^2)$. Next, sensing ranges in all other possible directions are determined based on an interpolation method. For simplicity, we use linear interpolation to specify the boundary of the sensing area. As an example, the approximation of the two representative nodes based on this model are shown in Figure 14. Clearly, our simplified model pretty accurately reflects the fluctuations of sensing ranges in different directions.

5.4 Robustness of Theoretical Predictions to Realistic Sensing Model

We now incorporate the realistic sensing range model into simulations to test the robustness of the performance predictions to sensing irregularity. We scaled the normal distribution $N(217, 32^2)$ to $N(10, 1.47^2)$ to fit the simulation setting. We use the same formulas as the previous idealistic experiments. The CDF's of detection delay under different parameter settings are shown in Figure 15. To illustrate the difference, we also plot the error relative to theoretical predictions in Figure 16.

We have two observations regarding these results. First, for our simulation settings, sensing irregularity has a very small effect. One primary reason is that even though the detection ranges do vary with different directions, the overall degree of coverage for the area remains almost the same, approximated by λ. Therefore, the overall detection delay distribution is almost not affected. Second, we observe that the maximal error relative to theoretical predictions is no more than 1.2%. As an example to show its implications, suppose that we have a set of system parameters that guarantees that 99% of intruding targets are detected within a certain time. Then, the actual detection rate should be no less than 97% with the existence of irregularity. Based on this observation, we conclude that our model is quite robust to realistic sensing conditions.

At last, we acknowledge that so far, our modeling of the realistic sensing model is only concerned with PIR sensors. Other types of sensors may well exhibit different characteristics, therefore, may have varied effect on the detection performance. However, we envision that with a relatively large system with considerable density, the effect of sensing irregularity will be considerably limited, leading to improvements in the accuracy of the aforementioned results.

6 Related Work

Research on minimizing energy consumption [5, 7, 8, 15, 18, 25, 28] has been one central topic in the sensor network community in recent years. Various effective techniques have been proposed, evaluated and implemented. Protocols to schedule nodes while maintaining full coverage have been proposed by [27, 14, 21, 10, 23]. The full sensing coverage model is very suitable for areas where continuous vigilance is required, but

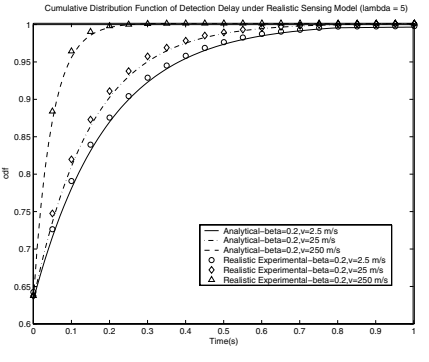

Fig. 15. Realistic Sensing Effect

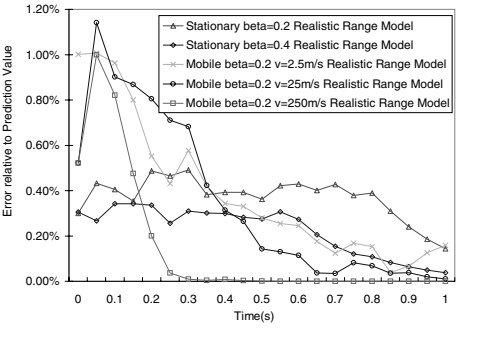

Fig. 16. Robustness of Theoretical Predictions

consumes considerable energy. There exists a lower bound on the minimal energy consumption if the requirement of full sensing coverage is to be fulfilled. To guarantee a longer sensor network lifetime, in certain situations, the designer may wish to keep partial sensing coverage in exchange of longer product lifetime.

Another related research direction is tracking and surveillance [2, 3, 4, 12, 13, 19, 20, 22, 26]. In these efforts, various tracking approaches are examined to optimize the overall surveillance quality. In particular, recent research efforts [9, 17, 11] have turned attention to the study of target tracking in the context of partial sensing coverage. In [9], the authors proposed the metric of quality of surveillance, which is defined as the average traveled distance of the target before it is detected. This is consistent with the model in our paper, where the average detection delay rather than distance is used. However, the authors didn't address the precise determination of this metric. Instead, they used an approximation model based on coverage process theory. Their attention is mainly focused on evaluating various sleep models with respect to the average travel length, which lead to considerably different results compared with ours. The work in [17] considers an equivalent problem to the type II target detection in our paper. However, we are more interested in deriving closed-form expressions for all four scenarios, whereas [17], while valuable, only considers fast targets and does not present closed-form results for detection delay. Another interesting work is [11], which considered the effect of different random and coordinated scheduling approaches, but provides no closed-form results. Therefore, we believe our work is a necessary complement towards thorough understanding of detection delay performance.

7 Conclusion and Future Work

This paper is the first to derive closed-form formulas for the distribution and expectation of detection delay for both stationary and mobile targets, and is also the first to propose and evaluate a realistic sensing model for sensor networks, to the best of the authors' knowledge. Extensive simulations are conducted and the results show the validity of the analysis. The analytical results are highly important for designers of energy efficient sensor networks for monitoring and tracking applications. Designers can apply these formulas to predict the detection performance without costly deployment and testing. Based on these formulas, they can make decisions on key system or protocol parameters, such as the network density and the duty cycle, according to the detection requirements of the system. Therefore, this work is a major contribution towards a thorough understanding of the relationship between system and protocol parameters and achievable detection performance metrics.

In the future, we intend to apply our results in large scale experiments. We also intend to expand our analysis to more irregular movement models, such as random waypoint movement. We hope the results can give us further insight on the fundamental tradeoffs in sensor network detection performance.

Acknowledgements

This work is supported in part by NSF grant CCR-0098269, ITR EIA-0205327 and CCR-0325197, the MURI award N00014-01-1-0576 from ONR, and the DARPA IXO offices under the NEST project (grant number F336615-01-C-1905).

References

1. In *http://www.cast.cse.ohio-state.edu/exscal/*.
2. J. Aslam, *et al.* Tracking a moving object with a binary sensor network. In *ACM Sensys*, 2003.
3. M. Batalin, *et al.* Call and response: Experiments in sampling the environment. In *ACM Sensys*, 2004.
4. K. Chakrabarty, *et al.* Grid coverage for surveillance and target location in distributed sensor networks. In *IEEE Transaction on Computers, 51(12)*, 2002.
5. B. J. Chen, *et al.* Span: An energy-efficient coordination algorithm for topology maintenance in ad hoc wireless networks. In *ACM Mobicom*, 2002.
6. CrossBow. In *http://www.xbow.com*.
7. D. Ganesan, *et al.* Power-efficient sensor placement and transmission structure for data gathering under distortion constraints. In *Proceedings of IPSN*, 2004.
8. L. Gu and J. Stankovic. Radio-triggered wake-up capability for sensor networks. In *IEEE RTAS*, 2004.
9. C. Gui and P. Mohapatra. Power conservation and quality of surveillance in target tracking sensor networks. In *ACM Mobicom*, 2004.
10. T. He, *et al.* An energy-efficient surveillance system using wireless sensor networks. In *ACM Mobisys*, 2004.
11. C. Hsin and M. Y. Liu. Network coverage using low duty-cycled sensors: Random and coordinated sleep algorithms. In *Proceedings of IPSN*, 2004.
12. J. J. Liu, *et al.* Distributed group management for track initiation and maintenance in target localization applications. In *Proceedings of IPSN*, 2003.
13. S. Megerian, *et al.* Exposure in wireless sensor networks. In *ACM Mobicom*, 2001.
14. S. Meguerdichian, *et al.* Coverage problems in wireless ad-hoc sensor networks. In *IEEE Infocom*, 2001.
15. S. Pattem, *et al.* Energy-quality tradeoff for target tracking in wireless sensor networks. In *Proceedings of IPSN*, 2003.
16. S. Port. *Theoretical Probability for Applications*. John Wiley and Sons,Inc, 1994.
17. S. Ren, *et al.* Analyzing object tracking quality under probabilistic coverage in sensor networks. In *ACM Mobile Computing and Communications Review*, 2005.
18. V. Shnayder, *et al.* Simulating the power consumption of large-scale sensor network applications. In *ACM Sensys*, 2004.
19. G. Simon, *et al.* Sensor network-based countersniper system. In *ACM Sensys*, 2004.
20. R. Szewczyk, *et al.* An analysis of a large scale habitat monitoring application. In *ACM Sensys*, 2004.
21. D. Tian, *et al.* A node scheduling scheme for energy conservation in large wireless sensor networks. In *Wireless Communications and Mobile Computing Journal*, 2003.
22. G. Veltri, *et al.* Minimal and maximal exposure path algorithms for wireless embedded sensor networks. In *ACM Sensys*, 2003.
23. X. R. Wang, *et al.* Integrated coverage and connectivity configuration in wireless sensor networks. In *ACM Sensys*, 2003.
24. E. W. Weisstein. Kolmogorov-smirnov test. In *MathWorld at http://mathworld.wolfram.com/Kolmogorov-SmirnovTest.html*.
25. J. Wu and M. Gao. On calculating power-aware connected dominating sets for efficient routing in ad hoc wireless networks. In IEEE ICPP, 200l.
26. N. Xu, *et al.* A wireless sensor network for structural monitoring. In *ACM Sensys*, 2004.
27. T. Yan, *et al.* Differentiated surveillance for sensor networks. In *ACM Sensys*, 2003.
28. F. Ye, *et al.* Peas:a robust energy conserving protocol for long-lived sensor networks. In *IEEE International Conference on Distributed Computing Systems(ICDCS)*, 2003.